AD-A108 676 AIR FORCE GEOPHYSICS LAB HANSCOM AFB MA F/G 14/2
WIND TUNNEL AND LABORATORY CALIBRATION OF BALLOON-BORNE WIND SE--ETC(U)
JUL 81 J H BROWN, R E GOOD
UNCLASSIFIED AFGL-TR-81-0219 NL

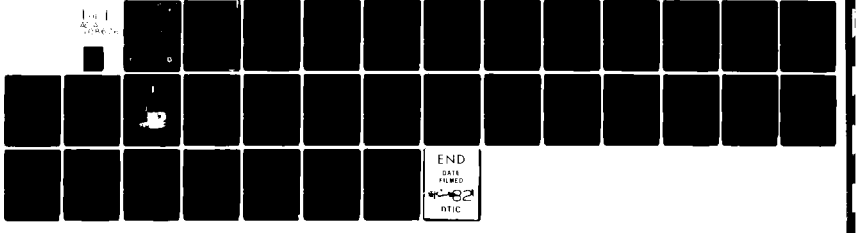

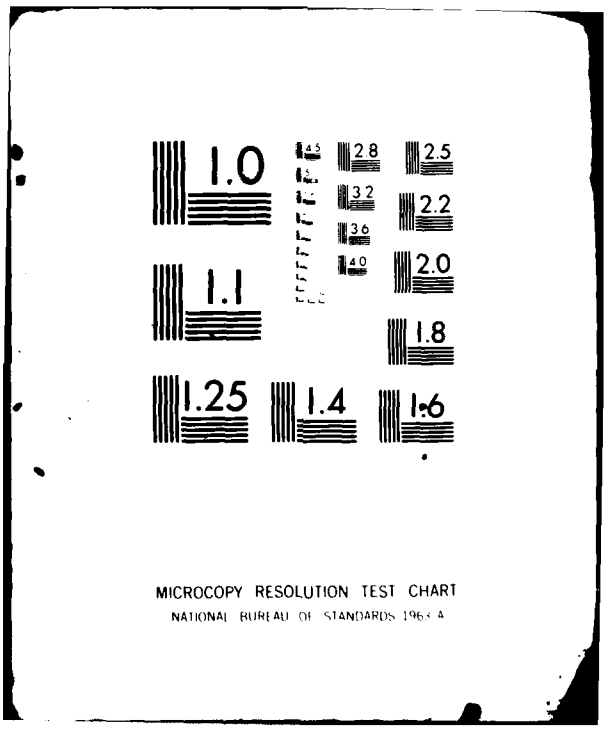
1.0
1.1
1.25
1.4
1.6
1.8
2.0
2.2
2.5
2.8
3.2
3.6
4.0
4.5
MICROCOPY RESOLUTION TEST CHART
NATIONAL BUREAU OF STANDARDS 1963 A

LEVEL II

12

AFGL-TR-81-0219
INSTRUMENTATION PAPERS, NO. 303

Wind Tunnel and Laboratory Calibration of Balloon-Borne Wind Sensors

J. H. BROWN
R. E. GOOD

27 July 1981

AERONOMY DIVISION PROJECT 6687
AIR FORCE GEOPHYSICS LABORATORY
HANSCOM AFB, MASSACHUSETTS 01731

AIR FORCE SYSTEMS COMMAND, USAF

This report has been reviewed by the ESD Information Office (OI) and is releasable to the National Technical Information Service (NTIS).

This technical report has been reviewed and
is approved for publication.

FOR THE COMMANDER

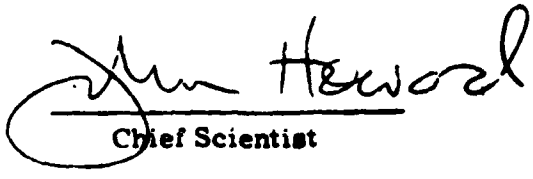

Chief Scientist

Qualified requestors may obtain additional copies from the Defense Technical Information Center. All others should apply to the National Technical Information Service.

Unclassified

SECURITY CLASSIFICATION OF THIS PAGE (When Data Entered)

REPORT DOCUMENTATION PAGE	READ INSTRUCTIONS BEFORE COMPLETING FORM
1. REPORT NUMBER AFGL-TR-81-0219	2. GOVT ACCESSION NO. AD-A105 676
	3. RECIPIENT'S CATALOG NUMBER
4. TITLE (and Subtitle) a WIND TUNNEL AND LABORATORY CALIBRATION OF BALLOON-BORNE WIND SENSORS	5. TYPE OF REPORT & PERIOD COVERED Scientific. Interim
	6. PERFORMING ORG. REPORT NUMBER IP No. 303
7. AUTHOR(s) J. H. Brown R. E. Good	8. CONTRACT OR GRANT NUMBER(s)
9. PERFORMING ORGANIZATION NAME AND ADDRESS Air Force Geophysics Laboratory (LKD) Hanscom AFB Massachusetts 01731	10. PROGRAM ELEMENT, PROJECT, TASK AREA & WORK UNIT NUMBERS 62101F 66870505
11. CONTROLLING OFFICE NAME AND ADDRESS Air Force Geophysics Laboratory (LKD) Hanscom AFB Massachusetts 01731	12. REPORT DATE 27 July 1981
	13. NUMBER OF PAGES 32
14. MONITORING AGENCY NAME & ADDRESS(if different from Controlling Office)	15. SECURITY CLASS. (of this report) Unclassified
	15a. DECLASSIFICATION DOWNGRADING SCHEDULE

16. DISTRIBUTION STATEMENT (of this Report)

Approved for public release; distribution unlimited

17. DISTRIBUTION STATEMENT (of the abstract entered in Block 20, if different from Report)

18. SUPPLEMENTARY NOTES

19. KEY WORDS (Continue on reverse side if necessary and identify by block number)

Corona	Calibration
Velocity	Stratosphere
Wind tunnel	Balloon
Ion drift	Turbulence

20. ABSTRACT (Continue on reverse side if necessary and identify by block number)

Two low-speed wind sensors have been calibrated for measuring the wind speed at an instrument suspended below stratospheric balloons. The low Reynolds number environment was duplicated at the NASA/Ames low-speed MARSWIT wind-tunnel facility, and in a laboratory bell jar. The two new instruments are the time-of-flight instrument that measures the motion of an ion cloud through an open pipe, and the corona anemometer that measures the displacement of an ion beam transversing the air-stream flowing between two plates. The calibrations consist of placing the instruments in a flow stream,

DD FORM 1 JAN 73 1473 EDITION OF 1 NOV 65 IS OBSOLETE

Unclassified

SECURITY CLASSIFICATION OF THIS PAGE (When Data Entered)

and relating the instrument output to the flow-stream velocity. The laboratory calibration is easy to conduct, but is limited to a measurement of internal flow velocity. The wind-tunnel calibration is performed to relate laboratory calibration to freestream conditions.

Contents

Illustrations

Illustrations

Preface

The authors are indebted to the excellent support provided by John Borghetti, Ed Trzcinski, and Bruce McFaden in developing the instruments. The wind tunnel testing was accomplished with the assistance of William Borucki and Rod Leach of NASA/Ames.

Wind Tunnel and Laboratory Calibration of Balloon-Borne Wind Sensors

1. INTRODUCTION

The stratospheric environment can be altered adversely when man-made pollutants are present for long periods of time. How long such pollutants remain in the stratosphere is determined by natural diffusion, transport, and mixing processes. Numerous balloon-borne measurements have been conducted to understand the characteristics of the processes that transport pollutants from the stratosphere. These have been measurements of the vertical distribution of trace constituents and measurements of the vertical structure of winds, pressure, and temperature.

A new and direct approach to the measurement of stratospheric winds, wind shear, and turbulence has been made possible by the development of gaseous discharge sensors. Gaseous discharge sensors are particularly well suited to stratospheric measurements by the ease in which the discharge potential can be electronically servo-adjusted to maintain constant current flows over the large ambient density and temperature conditions existing between 12 km and 30 km. This electronic control of the operating conditions assures establishment and maintainability of uniform velocity and turbulence measurement sensitivity. A stratospheric wind and turbulence (SWAT) sensor has been designed and flown successfully on seven balloon flights in the stratosphere. The SWAT sensor employs a corona discharge to measure the horizontal wind speed and direction, relative to the instrument platform, and to measure the velocity fluctuations (turbulence) from

(Received for publication 21 July 1981)

DC to 1000 Hz. Corona discharges to measure wind speed have been built using various principles. Franzen, Fuchs, and Schmitz[1] used the change in collected corona current; Ohigashi, Hamamoto, and Tanabe,[2] and Barat[3] used two different techniques to measure the deflection of an ion beam; and Lilienfeld, Solon, and DiGiovanni[4] observed the drift of an ion cloud.

The SWAT anemometer measures wind speed and turbulence by sensing the deflection of an ion beam transverse to the wind. The SWAT sensor consists of a corona source generating a flow of ions from the corona plate to the target plate. The target plate is segmented into four quadrants. The ion stream diffuses outward as it transverses the air gap between the two plates. In still air, the current collected by each quadrant of the target plate is identical. With a wind blowing between the two plates, the ions are deflected downstream by the wind. The difference in current collected on the quadrants is resolved to indicate the wind speed and direction.

The second instrument, an ion time-of-flight (TOF) device, directly measures the one-dimensional mean wind component at high altitudes, and serves as an in-flight reference for the SWAT sensors. The TOF instrument measures the wind speed by observing the drift of an ion cloud from the originating source to a distant current collector. A description of the electronics for both these anemomenters appears in Ref. 5.

The sensors are suspended 200 m below the large balloon, and measure the wind at the instrument level relative to the wind at the balloon level. This wind speed difference is usually low, having a typical mean value of less than 10 m. per second. This low speed, combined with low stratospheric pressures, represents a unique, low Reynolds number condition rarely encountered in other situations. Typical Reynolds numbers per unit length are a few hundred per cm.

---

1. Franzen, B., Fuchs, W., and Schmitz, G. (1961) Zeit. fuer Flugurssenschaften, 9:347.

2. Ohigashi, S., Hamamoto, Y., and Tanabe, S. (1968) Bull. JSME (Japan) 11:1169.

3. Barat, Jean (1975) C. R. Acad. Sci., Paris B280:220.

4. Lilienfeld, Pedro, Solon, Leonard, and DiGiovanni, Hugo (1967) Rev. Sci. Instrum., 38:405.

5. Murphy, George P. (1981) New Techniques and Devices for Measuring Stratospheric Winds and Turbulence, AFGL-TR-81-0128, ADA102680.

2. SENSOR DESCRIPTION

2.1 SWAT Anemometer

A corona is an electrical breakdown of a gas that occurs where nonuniform electric fields are encountered. It can occur with asymmetrical electrode geometry such as point to plane, sphere to cylinder, or wherever sharp-edged or small radii electrodes appear. Breakdown is initiated by the high fields concentrated at one or both of the electrodes; but complete breakdown to an arc, at or near the corona threshold, is precluded by the weak field between the electrodes. The appearance of corona current at the threshold levels is usually unstable due to an insufficient number of triggering electrons. Above threshold, and at a current on the order of micro-amperes, steady corona is achieved. Here, an increase in corona current is nearly proportional to an increase in the discharge potential. This is the so-called Ohm's Law Regime in which the SWAT sensors operate most frequently. Beyond this region, current increases parabolically with the applied potential, and eventually results in a complete transient arc or spark breakdown. Tests performed with SWAT sensors reveal that steady corona on onset is achieved at tens of volts above threshold, and spark breakdown occurs at a few hundred volts above the onset level. Actual potential voltage values depend upon pressure, P, and electrode separation, d.

The basic theory of operation of the corona anemometer can be predicted from the corona theories developed by Loeb,[6,7] and McDaniel and Mason.[8] Corona anemometers have been developed by Franzen, Fuchs, and Schmitz[1] to measure turbulence in wind tunnels, and by Waletzko[9] to measure surface winds. A new development was required to adapt the corona sensor to measure stratospheric winds relative to the motion of a floating balloon, and to detect the existence of turbulence directly and measure the turbulent intensity.[10]

A schematic of the SWAT sensor is shown in Figure 1. The ions are generated in the electric field created between the high voltage applied to the fine

6. Loeb, Leonard B. (1960) Basic Processes of Gaseous Electronics, University of California Press, Los Angeles.

7. Loeb, Leonard B. (1965) Electrical Coronas, University of California Press, Los Angeles.

8. McDaniel, Earl W., and Mason, Edward A. (1973) The Mobility and Diffusion of Ions in Gases, John Wiley & Sons, New York.

9. Waletzko, J. A. (1975) A new ion displacement system to measure the two-dimensional wind vector, Tech. Conf. on Automated Meteor. Sys., Washington, D. C.

10. Good, R. E., Brown, J. H., and Harpell, G. (1978) Development of a Corona Anemometer for Measurement of Stratospheric Turbulence, AFGL-TR-0070, Hanscom AFB, MA ADA058960.

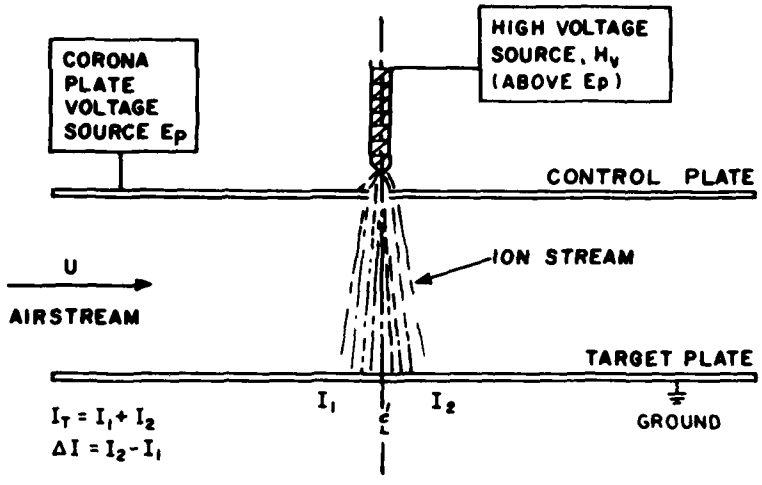

Figure 1. Schematic of Stratospheric Wind and Turbulence (SWAT) Sensor. The airstream velocity is measured as a function of the current difference collected at I_2 and I_1

needle point, and the lesser voltage applied to the control plate. A small, 0.64 cm diameter hole, on the centerline of the needle, typically allows 10% of the corona current to be drawn to the target plate. The voltage, E_p, applied to the control plate defines the rate of forced ion diffusion across the air gap. A high field will cause the ions to cross the air gap rapidly with little axial displacement or recombination. The field within the gap can be adjusted to set the velocity sensitivity of the SWAT sensor. When the sensor is operated with a constant current emitted from the needle, and a constant voltage applied to the control plate, the change in collected ion current between two adjacent quadrants is proportional to the wind component in that direction, provided that the air density remains constant. Variations in the air density change the ion recombination rates and the ion mobility, causing the total ion current incident upon the target plate to change. A needle of 90% platinum and 10% iridium metals, 0.6 mm diameter, ground to a sharp point, was found to achieve optimum compromise between sensitivity, life, and corona stability. There exists, however, an evolutionary history of the point that results in erosion of the point, with the consequent change in coronal characteristic and beam pattern. Also, the ion beam maintains a virtual origin at a spot on the needle that randomly wanders about the needle with time. These errors are minimized by providing a periodic zero-wind calibration. For this purpose, a shutter is closed over the air gap to achieve zero-wind condition. During this zero-wind condition an electronic servo loop automatically re-zeros the current sensing amplifier to allow the signal from each quadrant to be identical.

The SWAT sensor operates on the principle that the beam deflection is proportional to the freestream velocity as

$$\frac{\Delta E}{E_{TT}} = A \frac{V_\infty}{V_d} \tag{1}$$

where A is the proportionality constant, ΔE is the voltage representation of the ion current difference collected along either the X or Y axis of the target plate segmented into quadrants, E_{TT} is the voltage measurement of the total ion current it collected, V_∞ the airstream velocity, and V_d the ion drift velocity across the SWAT sensor. The drift velocity is found to be

$$V_d = K_o (E/\rho) \tag{2}$$

where K_o is the ion reduced mobility, ρ the ambient density, and E the local electric field strength (Volts/cm). The SWAT is operated with a field of Ep/L, with Ep=100 volts at pressures below 20 torr, and Ep=350 volts at higher pressures. The SWAT plate separation, L, is 2.54 cm. In practice, the SWAT sensor produces a processed output voltage, E_o, which is:

$$E_o = \frac{\Delta E}{E_{TT} P} \cdot \tag{3}$$

In terms of freestream velocity using Eqs. (1) and (2), E_o is

$$E_o = \left[\frac{A \ L \ \beta}{K_o \ E_p GRT}\right] \ V_\infty \tag{4}$$

where β represents the conversion between units, and R is the gas constant. The electrical gain, G, is switched as Ep is switched, to provide a suitable dynamic range of output. The bracketed quantity in Eq. (4) represents the calibration constant to be determined empirically. For each axis the SWAT electronics has four outputs. One channel contains an unfiltered low gain signal that has a flat frequency response out to 2 KHz. A second channel is amplified by a factor of 10 over the first channel. Two additional channels contain information that has been filtered through a 20 Hz high-pass filter, and amplified by factors of 10 and 100, respectively, over the low gain DC channel. This combination provides a dynamic range of 80 db for spectral analysis of the turbulent velocities.

2.2 TOF Anemometer

The TOF instrument is an open-ended flow tube with rounded entrances. An ion cloud, produced by a high-voltage, periodic pulse discharge at the upstream end of the flow tube, is carried by the airstream to a charge detector located 5.0 cm downstream. The discharge probe geometry consists of a 0.16 cm diameter ball at the end of a high-voltage lead placed inside a .635 cm OD open-ended stainless steel tube. The face of the tube is positioned at the centerline of the flow tube, and perpendicular to the flowstream. A negative high-voltage pulse, 600 - 2000 V, 75 ms wide, is applied to the ball once every second. A 32,000 Hz counter is triggered at the moment of discharge, and it is disabled when a peak detector senses the passing ion cloud. A shift register transmits the binary count that is converted directly to windspeed. The ion mass and the mass of an air molecule are nearly identical, so the ions acquire a velocity component parallel to the wind in a time period of a few collisions (t = 1-10 ns), which is small compared to the ion transit time.[4] Time measured for the ions to travel over a fixed distance is an accurate measure of the true windspeed within the flow tube. Accuracy is, however, affected by the determination of the travel distance, L, the molecular diffusion of the ion cloud, and the viscous flow conditions inside the tube. It is clear that, as the wind carries the ion cloud toward the charge collector, molecular diffusion and ion recombination reduce the amplitude of the charge distribution and broaden its Gaussian radius. At slow wind speeds, and low pressures, the ion density is changed significantly by the time the ions pass over the charge detector. Consequently, the sampled data appears skewed on the trailing side of the cloud. This does not affect the accuracy of the velocity determination for peak detection methods, except, at very low velocities, when the true peak is shifted several percent toward the early times.

3. CALIBRATION PROCEDURES

Several different calibration techniques have been developed to ascertain the correct velocity measurement. The fundamental calibration was performed in a low-density wind tunnel under simulated flight conditions. This calibration provides an absolute calibration, and relates the laboratory calibration to flight conditions. Laboratory calibration performed on each instrument relates the instrument's internal flow to instrumental output voltages. The laboratory calibration can be reproduced in flight using the known shedding frequency resulting[11] from air passing around the cylindrical supports at the entrance of the instrument.

---

11. Schlichting, H. (1969) Boundary-Layer Theory, McGraw-Hill, New York, p. 32.

Together, the three calibration techniques define the operational characteristics of the wind sensors.

3.1 Laboratory Calibrations

The entire sensor cannot be immersed in a low-density flow at the AFGL laboratory. It is necessary, therefore, to calibrate the instrument by simulating the flow through the instrument. In this procedure, the aerodynamic flow around the instrument is not simulated. A flow is produced inside the instrument and compared to the instrument response. Full-scale wind-tunnel measurements are required to relate the internal flow to the freestream flow. The laboratory measurements were performed inside an 18 in. bell jar held at the desired pressure. Flow was obtained by ducting the output of a squirrel-cage blower into the instrument (Figure 2). The airflow through the duct was measured with a Pitot probe using corrections for low Reynolds number conditions.[12] The airflow was adjusted by varying the squirrel-cage blower over a range of rotational speeds. The rotation rate of the 24-blade fan was determined by observing the rate blades interrupted a light beam. The mass flow through the duct was determined to be a unique function of the blower speed and bell jar pressure. Figures 3a and 3b represent the calibration data for the duct flow speeds at the location of the sensor. When the SWAT instrument is being calibrated, the SWAT walls form a part of the blower duct wall. The flow is, therefore, continuous through the duct and SWAT instrument. The SWAT instrument is inserted into the duct and located inside the bell jar for calibration (Figure 2). The bell jar is then pumped down several times to below 1 Torr pressure, recharging each time with dry air. Dry air is then admitted to the desired test pressure, and the blower speed is set to begin the flow-speed calibration.

The SWAT instrument was operated at two control plate voltages of Ep=100 and 350 volts. The output voltage as a function of bell-jar velocity follows a near constant relationship. The results are shown in Figures 4 and 5 for the two E_p conditions. The output voltage, E_o, is plotted as a function of the pressure and velocity inside the duct in order to separate the data taken at the different pressure conditions. For each pressure-test condition, the output voltage is a linear

12. Bryer, D., and Parkhurst, R. C. (1971) Pressure-Probe Methods for Determining Wind Speed and Flow Direction, National Physics Laboratory, London: Her Majesty's Stationery Office, p. 9.

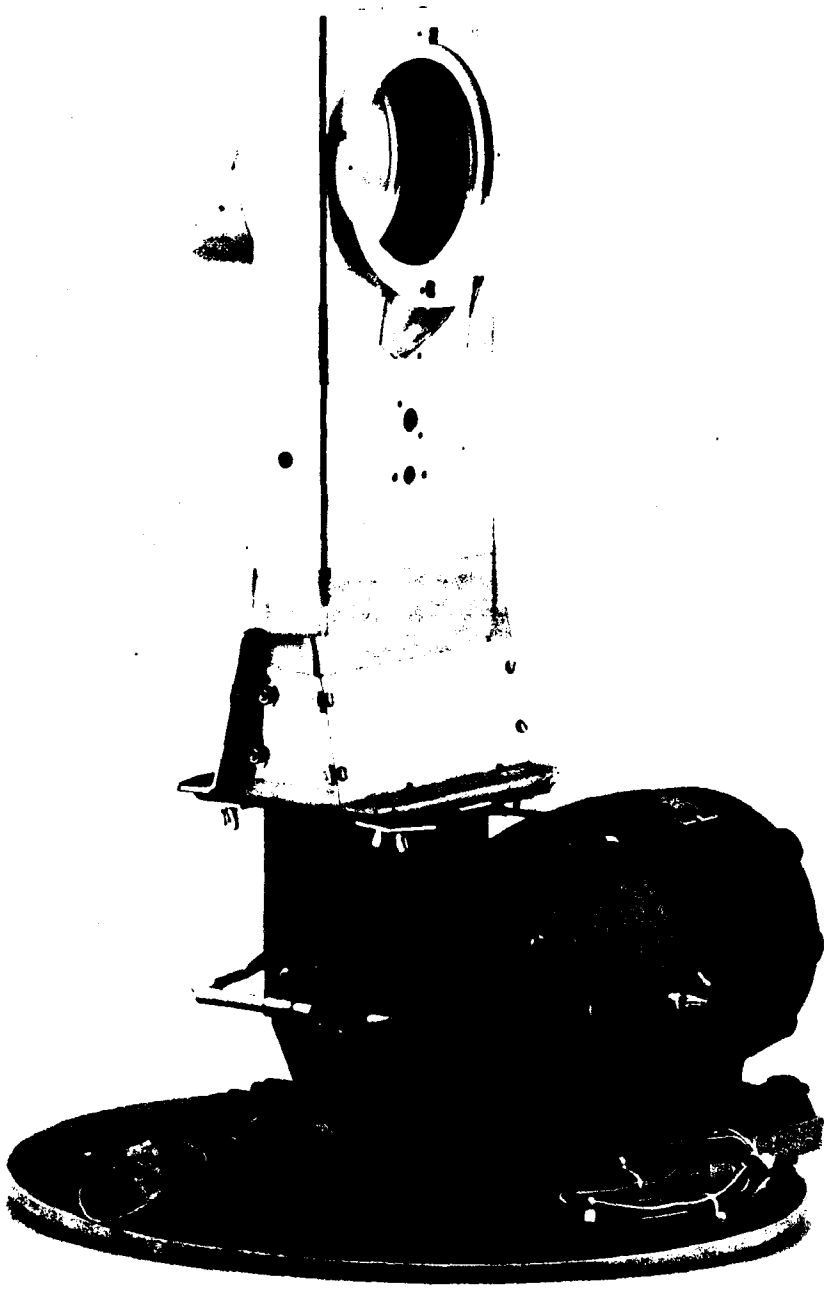

Figure 2. The Squirrel-Cage Blower and Duct are Shown as Used Inside the Eighteen-Inch Bell Jar

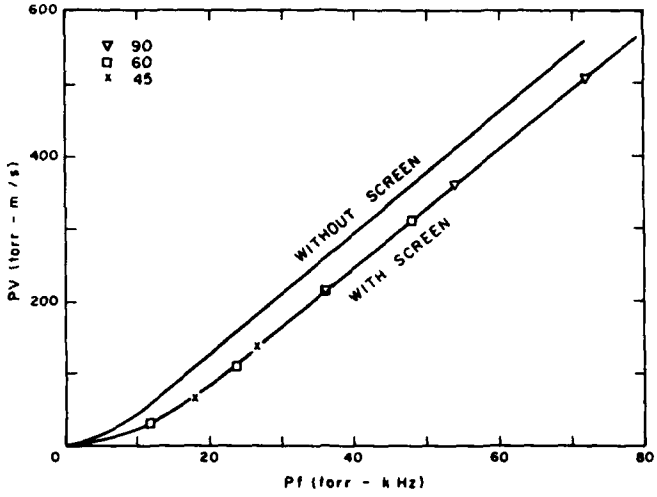

Figure 3a. The Velocity Through the Duct, Measured at the SWAT Sensor Station, is Monitored as a Function of Blower Speed. The blower speed is proportional to the rate the blower blades interrupt a light beam, measured as kilohertz. Two flow conditions exist; with and without a screen between the blower and the SWAT sensor

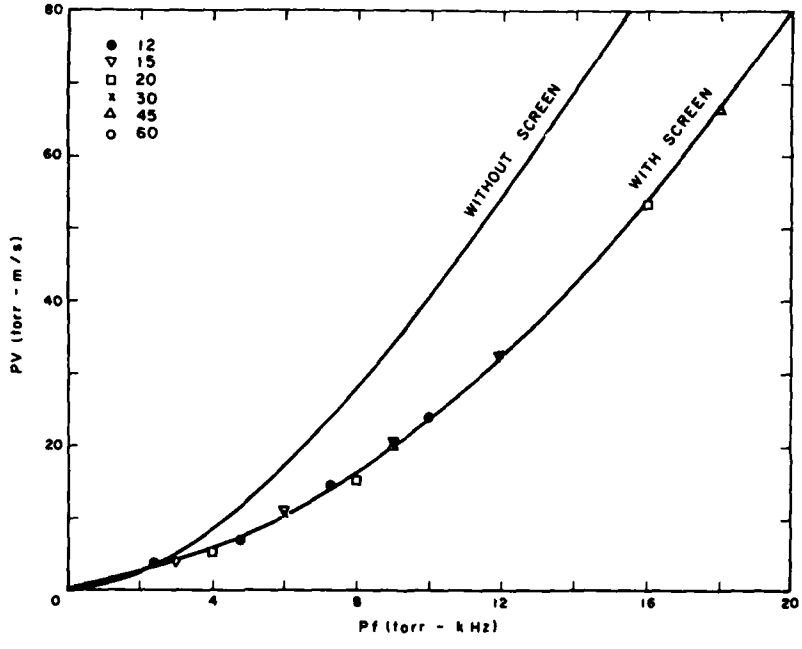

Figure 3b. Low-Velocity Conditions Obtained With the Squirrel-Cage Blower. Conditions as defined in Figure 3a

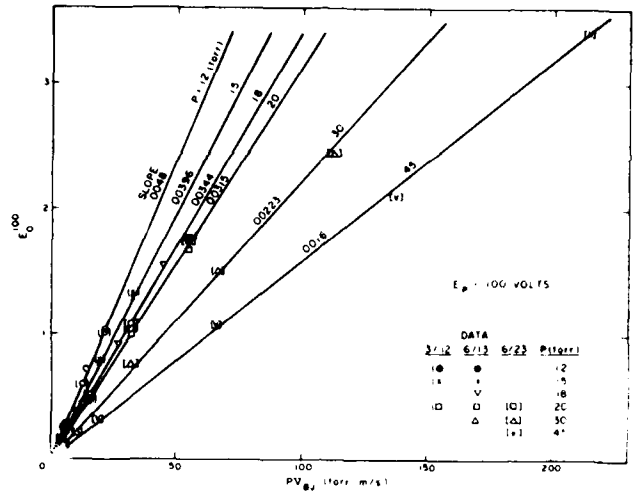

Figure 4. Bell-Jar Calibration of SWAT Sensor Showing the Sensor Voltage Output, E_o^{100}, as a Function of Pressure and Velocity. The SWAT sensor is operated at a field voltage E_p=100 volts

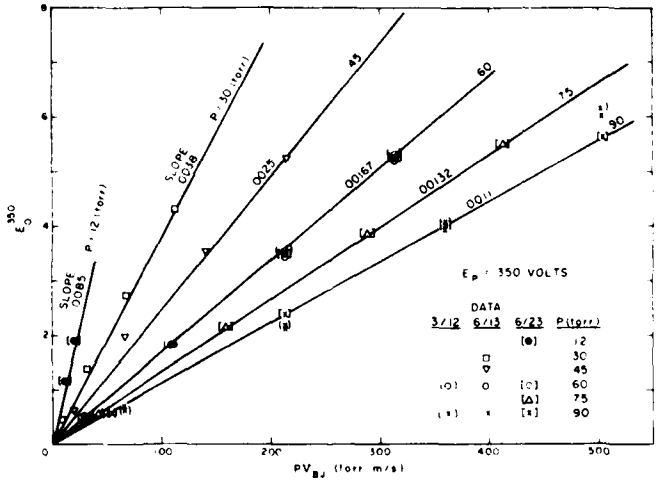

Figure 5. Bell-Jar Calibration of SWAT Sensor Showing the Sensor Voltage Output, E_o^{350}, as a Function of Pressure and Velocity. The SWAT sensor is operated at a field voltage of E_p=350 volts

function of PV as

$$E_o = S \cdot (PV) \tag{5}$$

where S is the slope. The slope varies with pressure, and is plotted in Figure 6 for all the test conditions. For the two plate voltages, the slope determined from bell-jar calibration is

$$S_{BJ}^{100} = .0366P^{-.82} \tag{6}$$

$$S_{BJ}^{350} = 0.1P^{-1} \tag{7}$$

combining Eqs. 6 and 7 with Eq. 5, the bell-jar calibration of the SWAT output voltage is given as

$$E_o^{100} = 0.037\ P^{.18}V_{BJ} \qquad E_p = 100 \text{ volts} \tag{8}$$

$$E_o^{350} = 0.1V_{BJ} \qquad E_p = 350 \text{ volts} \tag{9}$$

where V_{BJ} is the velocity inside the duct passing through the SWAT as measured by a Pitot probe. The weak pressure dependence observed at Ep=100 volts is assumed to be related to the non-linear effects of the high fields penetrating through the corona hole in the upper SWAT plate.

3.2 TOF Bell-Jar Calibration

The TOF sensor could not be tested directly inside the bell jar, since the TOF was larger than the blower duct. An alternative was to remove the spark source and the collector cathodes, and install them in the blower duct. In this manner, the flow speed measured by the Pitot probe and by the time-of-flight of the ion cloud could be compared. The ion cloud in the TOF instrument is subject to molecular diffusion and ion recombination. With a discharge current of 1 mA, 1×10^{-9} amps to 10^{-11} amps are collected at pressures of 10 mm Hg and 100 mm Hg, respectively, and velocity of 2 m/s. The cathode is a fine wire (.074 cm diam) placed into the flow tube perpendicular to the flow stream, and it is given a -10.0 volt DC potential. This is insufficient to cause resolvable ion acceleration, but it improves the received signal by attracting the positive ions in its vicinity, and repelling negative ions and electrons. By the time the ions have been carried to the collector, the 50 μs initial pulse time width of the ion

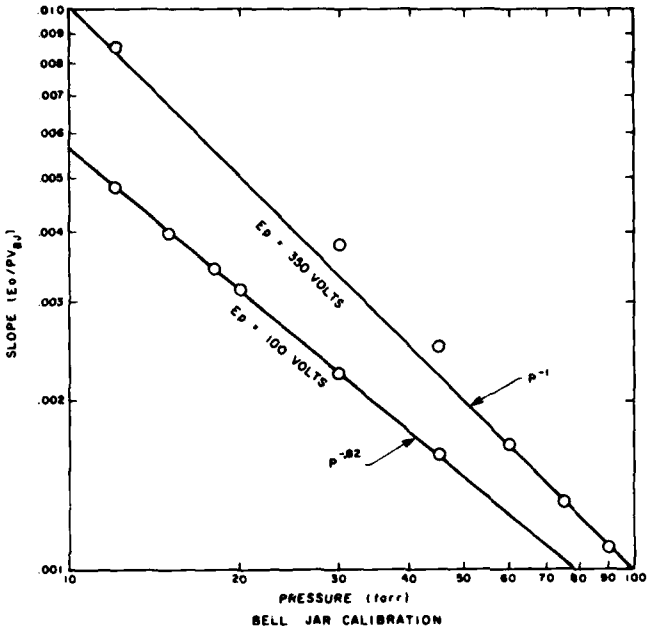

Figure 6. Pressure Dependence of the SWAT Calibration Performed in the Bell Jar. The slope is the ratio of $E_o/P\ V_{BJ}$ obtained from Figures 4 and 5

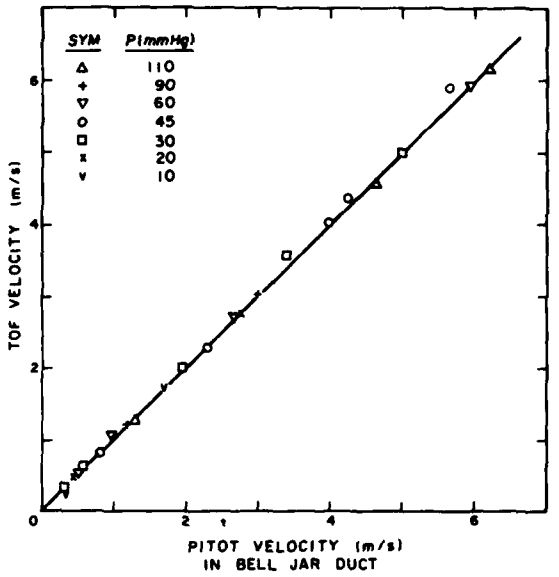

Figure 7. Comparison of Air Velocity Measured With the Time-of-Flight (TOF) Probes in the Bell-Jar Duct With the Air Velocity Measured With Standard Pitot Probe

cloud has spread to 1 ms when operating at a pressure of 10 mm Hg and a speed of 10 m/s. The spreading and recombination of the charge distribution, and being carried along by the wind, causes the detected signal to appear skewed on the trailing edge of the cloud, particularly at low speeds. This precludes determining the peak by means of measuring the arrival of a certain threshold current at the leading and trailing edges of the cloud and converting these times to an arithmetic average. Instead, a peak detector is used to measure the velocity to better than $0.1 m \cdot s^{-1}$.

The bell-jar calibration results shown in Figure 7 demonstrate that the TOF technique is an accurate means of measuring the flow speed.

3.3 Wind-Tunnel Calibration

Full-scale simulation tests were conducted at NASA/Ames using their low-density wind tunnel built for Mars surface wind simulation.[13] Wind-tunnel tests are important in determining the aerodynamic relationship between the free-stream velocity and the flow that enters the sensors and is measured by the instruments. The flow blockage and entrance condition affect the fraction of freestream mass flow passing through the instrument.

The Ames low-pressure tunnel has a cross-section 1.2 m x 0.9 m. The tunnel is driven by high-pressure air ejected through a series of small orifice nozzles located in the outlet diffuser section. Uniform flow exists in the tunnel. The sensors to be tested were located on the flow centerline, outside the tunnel-wall boundary layer. The tunnel was operated over the following conditions:

Velocity	1 to 20 m/s
Pressure	12 to 90 Torr
Temperature	~ 300 k

Both the TOF and SWAT sensors were calibrated, individually and side by side. In each instance, the tunnel flow was determined with Pitot probe measurements near the same station as the sensors.

3.3.1 TOF Results

Two probes of different inside diameters, 1 in. and 4 in., were tested to determine the effect of wall thickness to diameter ratio on the loss of flow speed inside the probes. The size of the two probes is given in Figure 8. The inside flow speed can be less than the freestream speed due to the aerodynamic blocking

13. White, B. R. (1979) Turbulent Boundary Layers: Forced, Incompressible, Non-Reacting. Ed. H. W. Weber, ASME, New York, pp. 209-220.

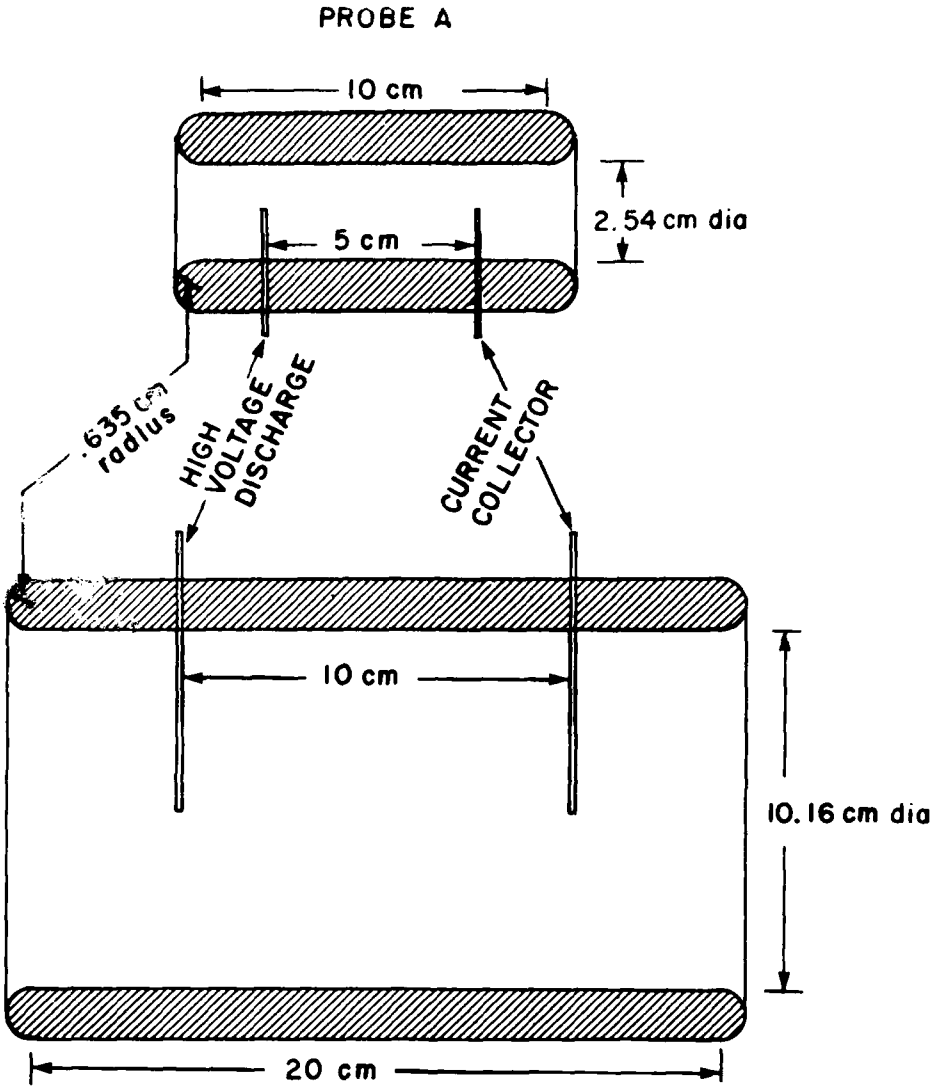

FIGURE 1

TIME-OF-FLIGHT WIND SPEED PROBES

Figure 8. Dimensional Drawing of the Two TOF Probes Studied. Probe A is the smaller probe with a 2.5 cm ID. Probe B is the larger probe with a 10.2 cm ID

of the flow. The results of the wind-tunnel measurements are shown in Figure 9. At least square fit to the data yields

$$V_\infty = (1.06 \pm .26)\, V_i \tag{10}$$

for the 4-in. probe and

$$V_\infty = (1.60 \pm .37)\, V_i \tag{11}$$

for the 1-in. probe where V_i is the velocity measured inside by the time-of-flight technique, and V_∞ is the tunnel freestream velocity.

The wind-tunnel measurements were conducted over Reynolds numbers ranging from 50 to 1500, based on the probe inside diameter, d. Of the 71 data points, only five were at Reynolds numbers greater than 1000. An attempt was made to observe a Reynolds number dependence using data in the Reynolds number range 100 to 900. Statistically significant Reynolds number dependence could not be obtained as an improvement over the straight line dependence on velocity shown above.

The velocity defect inside the probe is a result of the pressure forces on the inlet of the probe. Taking a momentum balance over a control volume surrounding the inlet,[14] the thrust on the inlet is $T = 1/2\, \rho / V_\infty^2\, (1-V_i/V_\infty)^2 - d^2/4$, where V_i is the internal velocity. The probe drag based on the frontal area is $D = 1/2\, \rho\, V_\infty^2\, \pi\, (d+t)tC_D$, where t is the probe wall thickness and C_D is the drag coefficient. Equating the thrust and drag, the velocity defect can be determined to first-order term as

$$\frac{\Delta V}{V_\infty} = 4 C_D \left(\frac{t}{d}\right) \left(1 + \frac{t}{d}\right) \tag{12}$$

where $\Delta V = V_\infty - V_i$. Using the wind-tunnel measurements, the average value of the drag coefficient is 0.045 and .0057 for probes A and B. The results indicate that the internal flow speed approaches the freestream speed when the probe wall thickness to diameter ratio is less than 0.1. In order to also have a well-rounded entrance to avoid entrance effects, and to minimize angle of attack effects, it is

14. Kuchemann, D., and Weber, J. (1953) Aerodynamics of Propulsion, 1st Ed., McGraw-Hill, New York, pp. 60-62.

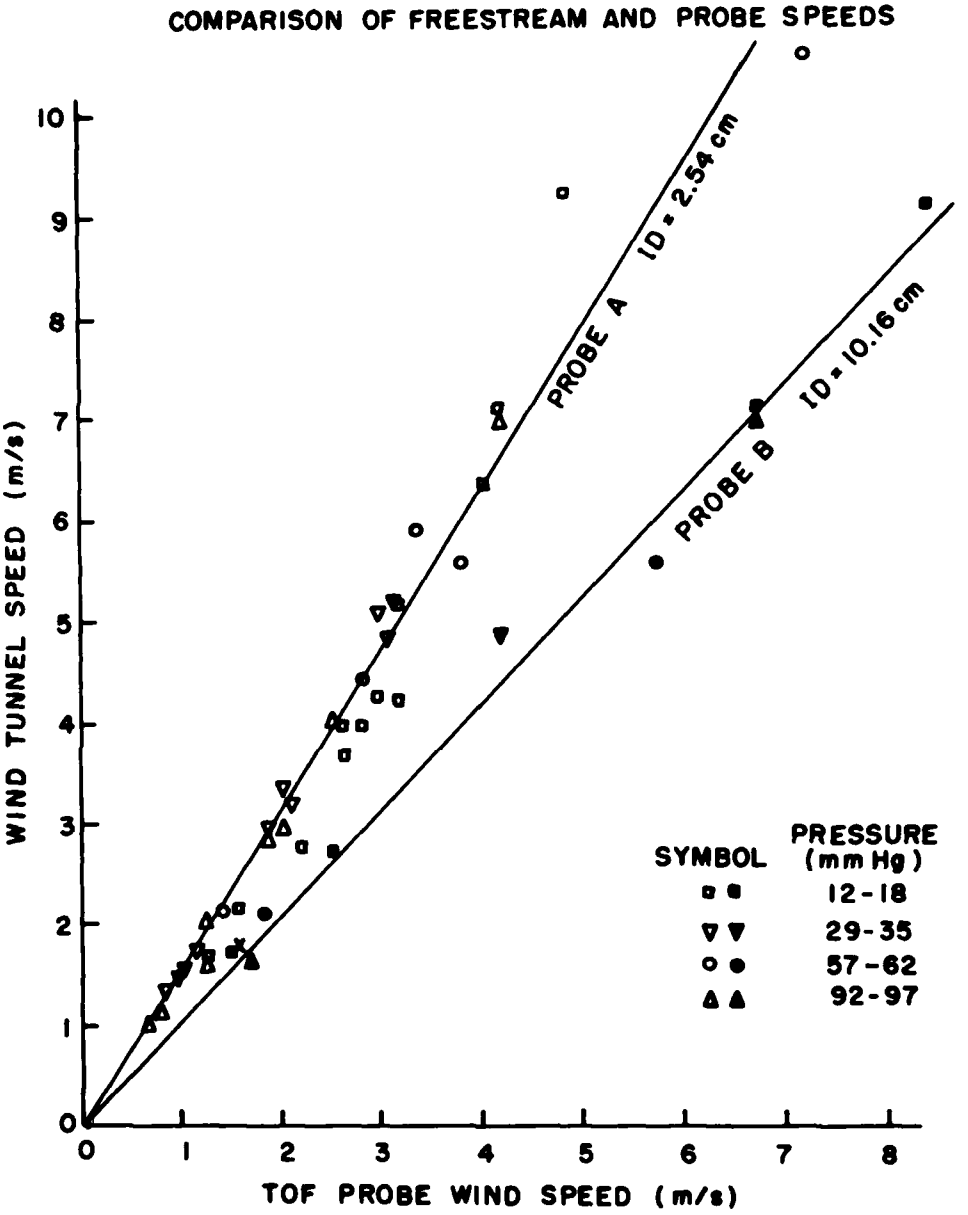

Figure 9. Wind-Tunnel Comparison of Freestream Velocity Measured by Pitot Probes With the Velocity Measured by TOF Probes A and B

necessary to utilize a large diameter probe. Thus the time-of-flight speed measurement inside a large diameter, thin-wall probe will measure freestream speed.

The angle-of-attack sensitivity was determined by mounting the probe on a rotatable table. The tunnel was operated at a constant velocity, while the TOF 1-in. probe was rotated ± 70 degrees with respect to the freestream velocity vector. The TOF velocity remained measurable constant over ± 27 degrees angle-of-attack. The flow inside the sensor decreased rapidly at angles greater than 27 degrees as shown in Figure 10. No change in the angular dependence was observed

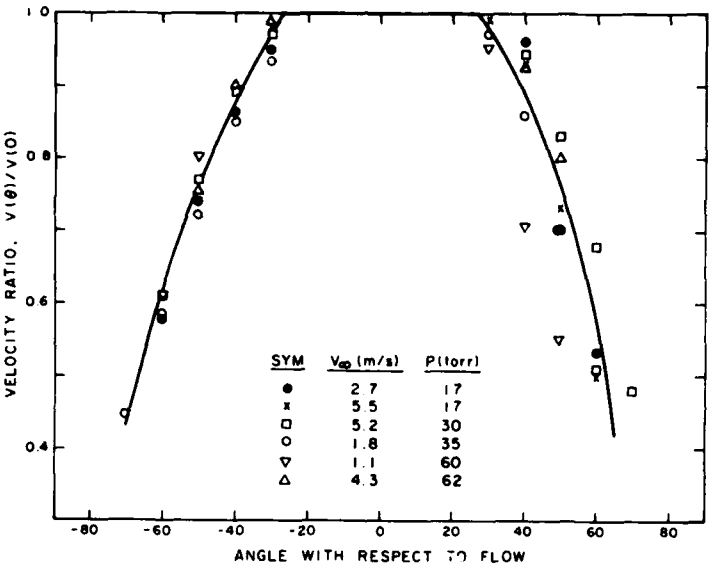

Figure 10. Angle-of-Attack Dependence of the TOF Probe A as Measured in the Wind Tunnel at Various Air Velocities

with pressure or velocity. An analytical expression for the velocity ratio at angles greater than 27 degrees is

$$V(\theta)/V(o) = 1 - 6.4 \times 10^{-3} X - 1.55 \times 10^{-4} X^2 \qquad (13)$$

where $X = \theta - 27$ and is valid only for $X > 0$.

The TOF is axisymmetrical and, therefore, the angular velocity dependence can be applied to both yaw and pitch, or any combination of the two.

An attempt was made to measure the freestream velocity through the use of freestanding spark source and a downstream current collector. At a separation distance of 10 cm, no detectable current could be collected. The pipe shroud around the probes hinders the radial diffusion of the ion cloud, making it possible to collect the current.

3.3.2 SWAT Results

The SWAT sensor was placed in the tunnel flow to determine the relationship of the measured flow speed to the freestream speed. The SWAT sensor was operated at the two control-plate voltages, E_p=100 and 350 volts, while the tunnel was operated over a range of pressures and velocities. Following the same procedure used in the bell-jar calibration, the SWAT output voltage, E_o, is plotted as a function of the wind-tunnel pressure velocity, and is shown in Figures 11 and 12. The slope of the linear curves is shown as a function of pressure (Figure 13). It is observed that the slope pressure dependence for

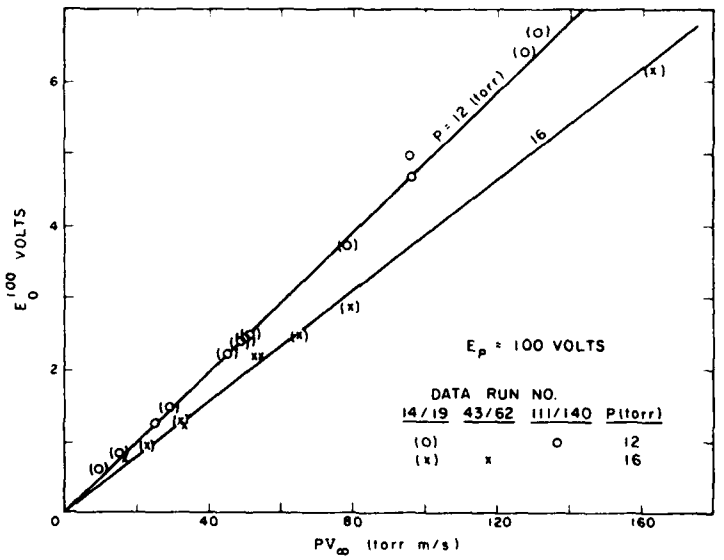

Figure 11. Wind-Tunnel Calibration of SWAT Sensor Showing the Sensor Voltage Output, E_o^{100}, as a Function of Pressure and Velocity. The SWAT sensor is operated at a field voltage of E_p=100 volts

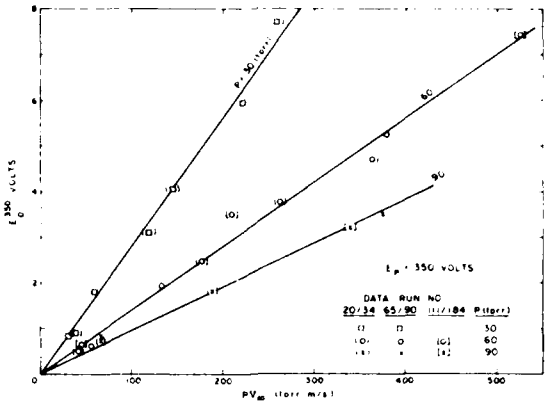

Figure 12. Wind-Tunnel Calibration of SWAT Sensor Showing the Sensor Voltage Output, E_o^{350}, as a Function of Pressure and Velocity. The SWAT sensor is operated at a field voltage of E_p=350 volts

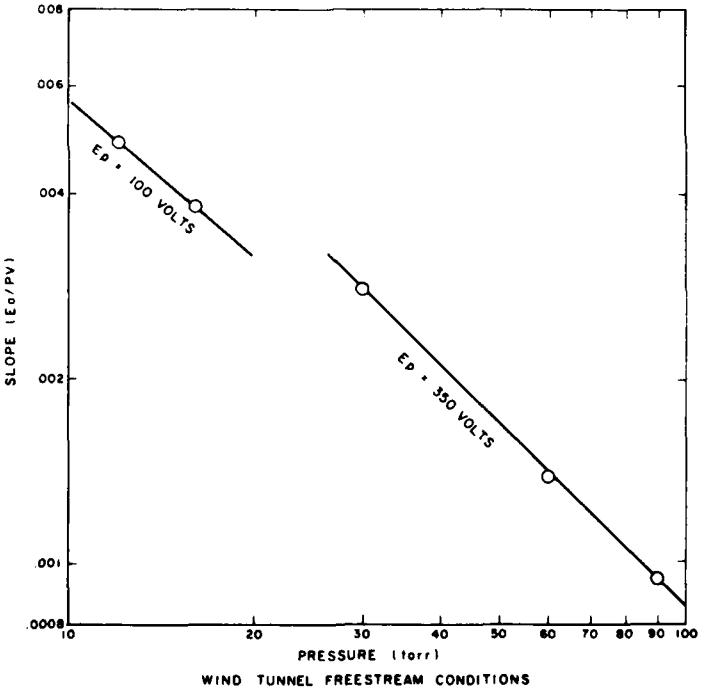

Figure 13. Pressure Dependence of the SWAT Calibration Performed in the Wind Tunnel. The slope is the ratio of $E_o/P\,V_{BJ}$ obtained from Figures 11 and 12

the two operating conditions is:

$$S_{\infty}^{100} = 0.033\ p^{-.82} \qquad E_p = 100 \tag{14}$$

$$S_{\infty}^{350} = 0.084\ p^{-1} \qquad E_p = 350\ . \tag{15}$$

The pressure dependence for the $E_p = 100$ volt case cannot be determined accurately with only the two pressure conditions used in the wind tunnel. Since the pressure dependence was well defined in the bell-jar calibration, the same pressure dependence is assumed to hold in the wind-tunnel environment. The output voltage, E_o, for the two operating conditions as determined from Figures 11-13 is is

$$E_o^{100} = 0.67\ P^{.18}\ V_{\infty} \qquad E_p = 100 \tag{16}$$

$$E_o^{350} = 0.084\ V_{\infty} \qquad E_p = 350\ . \tag{17}$$

No angle-of-attack measurements with the SWAT sensor were conducted in the wind tunnel. Previous aerodynamic testing[10, 15] has shown that the SWAT sensor having a 1/2 in. radius on the entrance surfaces was insensitive to angle-of-attack variation up to ± 30 degrees.

The SWAT sensor is designed to measure the instantaneous velocity, and thereby provide information on ambient turbulence. An important question is, "Does the sensor generate turbulence internally?" If this were to occur, any ambient turbulence would be masked by instrument turbulence. The wind-tunnel experiments were used to answer this question. The wind tunnel is, unfortunately, not free of turbulence itself. Some smaller scale turbulence does remain in the wind tunnel since the flow is generated by a fan. Flow straighteners, located at the tunnel entrance, are used to smooth the flow. This reduces the large wind-speed fluctuations sometimes observed in Pitot probe readings.

Turbulence was studied by feeding one of the ac output channels of the SWAT sensor into a Nicolet Spectrum Analyzer, Model 440A. The relative power spectral density (PSD) obtained as a function of frequency is shown in Figures 14 and 15 for 13 mm Hg and 16 mm Hg pressure conditions. When turbulence is present the PSD increases in amplitude and extends to higher wavenumbers. Two examples of PSD versus wavenumber are shown in Figures 16 and 17 for pressures 13 mm Hg and 29 mm Hg. In wave space, it can be seen that the turbulence level, at wave-

15. Durgin, Frank H., and Fanucci, Jerome P. (1977) Static and Dynamic Calibration of a Corona Discharge Anemometer, AFGL-TR-77-0022, ADA040038.

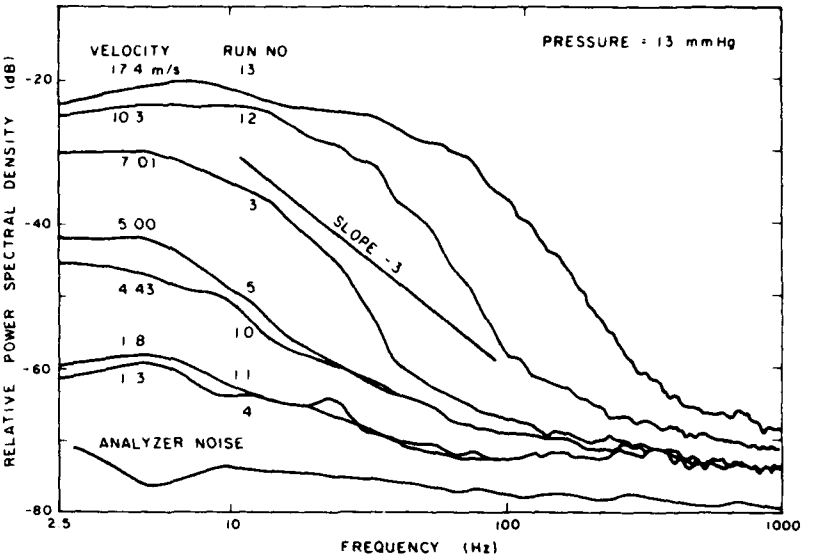

Figure 14. Power Spectral Analysis of SWAT Data in Frequency Space for Various Wind-Tunnel Velocities at a Pressure of 13 mm Hg

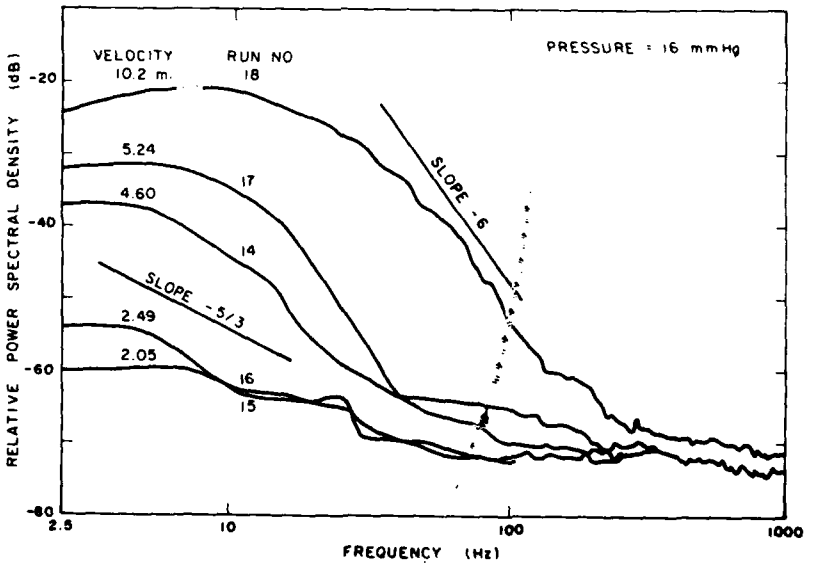

Figure 15. Power Spectral Analysis of SWAT Data in Frequency Space for Various Wind-Tunnel Velocities at a Pressure of 16 mm Hg.

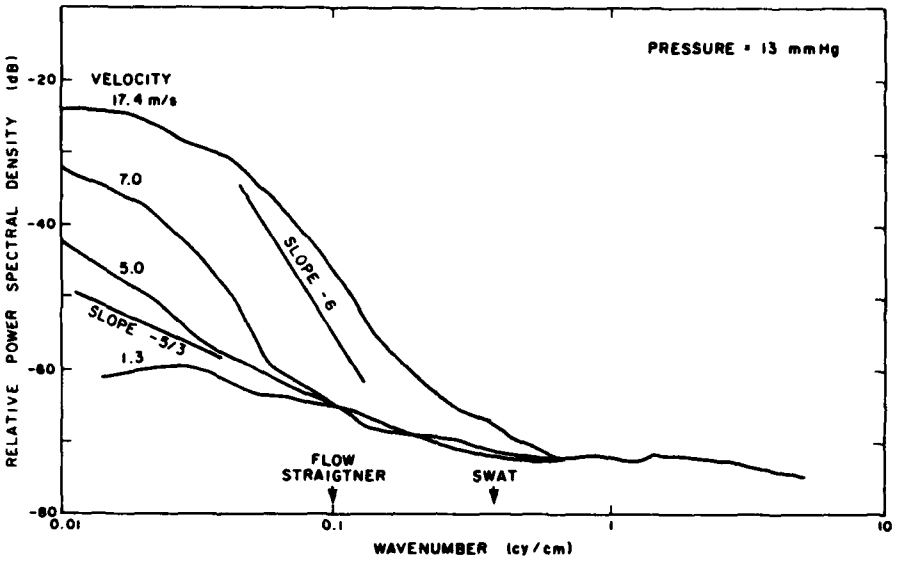

Figure 16. Power Spectral Analysis of SWAT Data in Wave Space for Various Wind-Tunnel Velocities at a Pressure of 13 mm Hg. A -5/3 slope occurs up to a velocity of approximately 5 m/s. Higher velocities yield power spectrum with a -6 slope

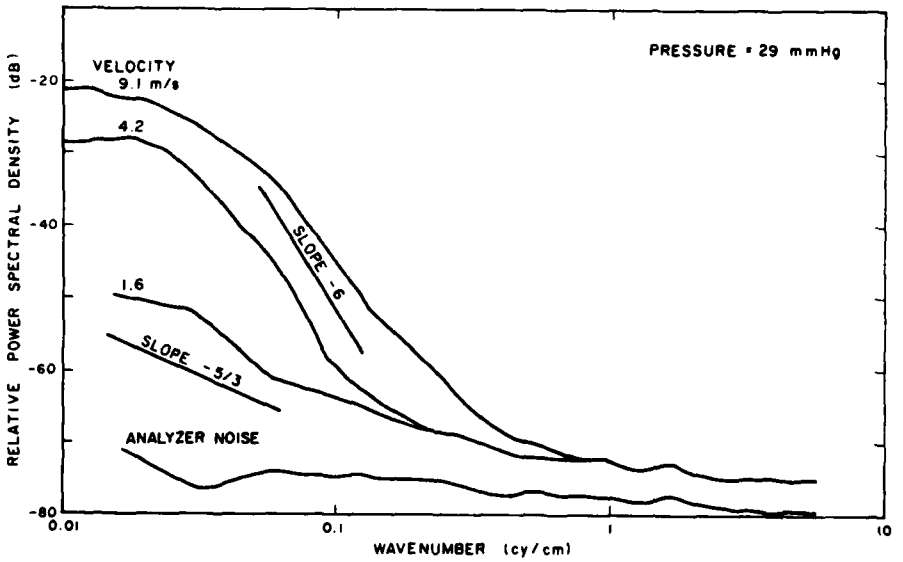

Figure 17. Power Spectral Analysis of SWAT Data in Wave Space for Various Wind-Tunnel Velocities at a Pressure of 29m mm Hg. A -5/3 slope occurs up to a velocity of approximately 1.6 m/s. Higher velocities yield power spectrum with a -6 slope

numbers greater than 0.08, are independent of velocity and are very low. The flow straightener, which forms a screen with 10 cm x 10 cm openings, has a wave number of 0.1 cycle/cm. The straightener is effective since the turbulence is suppressed. A velocity greater than 10 m/sec at 13 mm Hg pressure and 7 m/s at 29 mm Hg pressure is required to pass tunnel turbulence through the flow straightener. The wavenumber of the 1-in. opening in the SWAT sensor is also shown in Figure 16.

Wind-tunnel turbulence behind a screen is known to decay with distance from the screen, and to have a PSD slope of approximately -5/3. This is observed in Figures 16 and 17 at velocities less than 5 m/s and 2 m/s, respectively. At higher velocites, the slopes are much higher and approach -6. This implies that at higher velocities, the SWAT sensor generates turbulence that is dissipated locally. Thus, ambient turbulence can be detected only below certain velocity levels. An appropriate Reynolds number scaling, based on the above two observations, below which no internal turbulence is generated, is $Re/cm < 60\ cm^{-1}$.

4. ANALYSIS

Each SWAT sensor has a slightly different bell-jar calibration since the needle and needle position are shaped and positioned individually. It is necessary, therefore, to relate the bell-jar calibration performed on each SWAT sensor to the flight condition. The wind tunnel and bell-jar calibration presented in Section 2 serves as a model. They can be normalized to allow each subsequent bell-jar calibration to be related to an equivalent wind-tunnel calibration and, hence, the flight conditions.

The wind-tunnel tests show that the freestream wind speed can be related to the SWAT output as

$$V_\infty = E_o / P S_\infty \tag{18}$$

where the slope S_∞ is determined in wind-tunnel calibrations. The present tests provide the relationship between the wind-tunnel derived slope and the bell-jar derived slope as

$$S_\infty^{350} = 0.84\, S_{BJ}^{350} \tag{19a}$$

and

$$S_\infty^{100} = 0.89\, S_{BJ}^{100} \quad . \tag{19b}$$

The lower freestream slope implies that the flow is decelerated slightly inside the SWAT sensor, about 15%. Thus, for the SWAT, $V_\infty = 1.15V_{BJ}$ and

$$V_\infty = 1.15E_o/PS_{BJ} \tag{20}$$

Finally, the freestream wind-speed measurement can also be obtained with the TOF instrument using the calibration Eq. (10) or (11) depending upon the sensor physical dimensions. The SWAT sensor can be used to measure the wind speed using the calibration Eq. (20). This requires each SWAT instrument to be calibrated in the laboratory to determine the voltage to wind-speed calibration constant. This constant must be corrected further when operating in nonstandard temperatures using the dependence shown in Eq. (4).

References

1. Franzen, B., Fuchs, W., and Schmitz, G. (1961) Koronaanemometer zur messung von turbulenzkomponenten (Corona anemometer for the measurement of turbulent components), Zeitschrift fuer Flug Wissenschaften, 9(11):347-351 (November 1961).

2. Ohigashi, S., Hamamoto, Y., and Tanabe, S. (1968) Technique of measuring gas stream velocity by means of electric discharge, Japan Society of Mechanical Engineers Bulletin, 11(48):1169-1174 (December 1968).

3. Barat, Jean (1975) Étude expérimental de la structure du champ de turbulence dans la moyenne stratosphère (Experimental study of the turbulent field structure in the middle stratosphere.) Comptes Rendus Hebd. Seances Acad. Sci. B. (France) 280(22):691-693 (9 June 1975).

4. Lilienfeld, Pedro, Solon, Leonard R., and DiGiovanni Hugo J. (1967) Ion tracer anemometer for the measurement of low density air flow, Rev. Sci. Instrum., 38:405-409 (March 1967).

5. Murphy, George P. (1981) New Techniques and Devices for Measuring Stratospheric Winds and Turbulence, AFGL-TR-81-0128, ADA102680.

6. Loeb, Leonard B. (1960) Basic Processes of Gaseous Electronics, University of California Press, Los Angeles.

7. Loeb, Leonard B. (1965) Electrical Coronas, University of California Press, Los Angeles.

8. McDaniel, Earl W., and Mason, Edward A. (1973) The Mobility and Diffusion of Ions in Gases, John Wiley & Sons, New York.

9. Waletzko, J. A. (1975) A new ion displacement system to measure the two-dimensional wind vector, Tech. Conf. on Automated Meteor. Syst., Washington, D. C.

10. Good, R. E., Brown, J. H., and Harpell, G. (1978) Development of a Corona Anemometer for Measurement of Stratospheric Turbulence, AFGL-TR-78-0070, Hanscom AFB, MA ADA058960.

11. Schlichting, H. (1969) Boundary-Layer Theory, McGraw-Hill, New York, p. 32.

12. Bryer, D., and Parkhurst, R. C. (1971) Pressure-Probe Methods for Determining Wind Speed and Flow Direction, National Physics Laboratory, London: Her Majesty's Stationery Office, p. 9.

13. White, B. R. (1979) Turbulent Boundary Layers: Forced, Incompressible, Non-Reacting. Ed. H. W. Weber, ASME, New York, pp. 209-220.

14. Kuchemann, D., and Weber, J. (1953) Aerodynamics of Propulsion, 1st Ed., McGraw-Hill, New York, pp. 60-62.

15. Durgin, Frank H., and Fanucci, Jerome P. (1977) Static and Dynamic Calibration of a Corona Discharge Anemometer, AFGL-TR-77-0022, ADA040038.

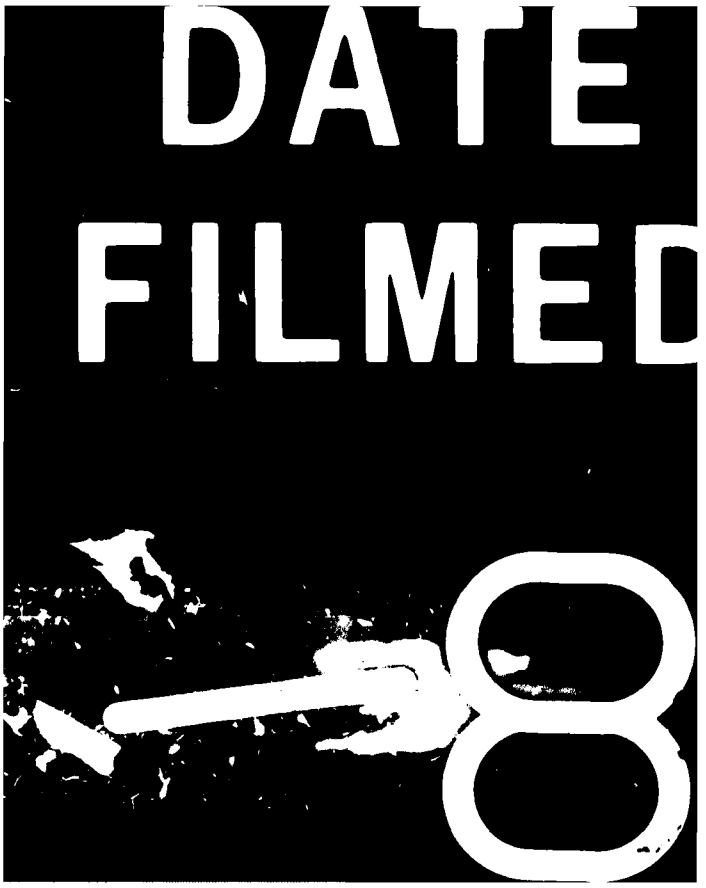
DATE
FILMED
8